NANO · MICRO small
www.small-journal.com

Toward Diffusion Measurements of Colloidal Nanoparticles in Biological Environments by Nuclear Magnetic Resonance

Daniel Padro, Philipp Cienskowski, Sonia Lopez-Fernandez, Indranath Chakraborty, Carolina Carrillo-Carrion, Neus Feliu, Wolfgang J. Parak, and Monica Carril**

Protein corona formation on the surface of nanoparticles (NPs) is observed in situ by measuring diffusion coefficients of the NPs under the presence of proteins with a ^{19}F nuclear magnetic resonance (NMR) based methodology. Formation of a protein corona reduces the diffusion coefficient of the NPs, based on an increase in their effective hydrodynamic radii. With this methodology it is demonstrated that the apparent dissociation constant of protein–NP complexes may vary over at least nine orders of magnitude for different types of proteins, in line with the Vroman effect. Using this methodology, the interaction between one type of protein and one type of nanoparticle can be studied quantitatively. Due to the NMR-based detection, this methodology has no interference by absorption/scattering effects, by which optical detection schemes are affected. By using the potential of the NMR chemical shift, the detection of multiple ^{19}F signals simultaneously opens the possibility to study the diffusion of several NPs at the same time. The ^{19}F labeling of the NPs has negligible effect on their acute toxicity and moderate effect on NPs uptake by cells.

1. Introduction

Engineered nanoparticles (NPs) for biomedical applications undergo spontaneous protein adhesion when placed in biological fluids, such as blood. This phenomenon is known as protein corona[1] and it has direct implications in the cellular uptake,[2] circulating times,[3] fate,[4] and toxicity[5] of NPs in living beings. Thus, in order to learn about the NPs' interaction with proteins and cells, in situ characterization would be helpful, that is, quantification methods without the need to isolate NPs from their environment. In situ characterization about the fate of NPs could for example help to unravel how the interactions of the NPs with biological matter affect in vivo toxicity.

The adhesion of proteins to NPs' surfaces is in general nonspecific, i.e., not mediated by specific chemical bonds. It is rather driven by electrostatic or hydrophobic forces between the NPs and the proteins, which means that the vast majority of NPs are subject to it. A number of techniques have been reported to study in situ changes in the original physicochemical properties of NPs after protein corona formation, many of which require the use of light. Examples are absorption spectroscopy,[6] fluorescence spectroscopy,[7] dynamic light scattering (DLS),[8] fluorescence correlation spectroscopy (FCS),[9] circular dichroism (CD),[10] etc. Optical methods can be very sensitive and easy to implement,[11] however, they have often limited translation to more complex environments, such as those encountered in vivo, due to light scattering. It has been recently demonstrated that diffusion coefficients of colloidal NPs can be determined with a non-optical detection technique based on nuclear magnetic resonance (NMR).[12] With this technique the adsorption of proteins to the surface of the NPs could be measured as a reduction in the diffusion coefficient of the NPs upon the presence of proteins, equivalent to an increase

Dr. D. Padro, Dr. C. Carrillo-Carrion, Prof. W. J. Parak
Center for Cooperative Research in Biomaterials (CIC biomaGUNE)
Basque Research and Technology Alliance (BRTA)
Paseo de Miramon 182, Donostia-San Sebastián 20014, Spain
E-mail: wparak@cicbiomagune.es

P. Cienskowski
BioNTech SE
Mainz 55131, Germany

The ORCID identification number(s) for the author(s) of this article can be found under https://doi.org/10.1002/smll.202001160.

DOI: 10.1002/smll.202001160

S. Lopez-Fernandez
Fundación Biofísica Bizkaia/Biofisika Bizkaia Fundazioa (FBB)
Leioa E-48940, Spain

S. Lopez-Fernandez, Dr. M. Carril
Instituto Biofisika UPV/EHU
CSIC
Barrio Sarriena s/n, Leioa, Bizkaia E-48940, Spain
E-mail: monica.carrilg@ehu.eus

Dr. I. Chakraborty, Dr. N. Feliu, Prof. W. J. Parak
Center for Hybrid Nanostructures
University of Hamburg
Hamburg 20146, Germany

Dr. M. Carril
Departamento de Bioquímica y Biología Molecular
UPV/EHU
Barrio Sarriena s/n, Leioa, Bizkaia E-48940, Spain

Dr. M. Carril
Ikerbasque
Basque Foundation for Science
Bilbao 48013, Spain

in effective hydrodynamic diameter due to the formation of a protein corona. Although the use of our NMR-based detection requires higher sample concentrations due to its lower sensitivity as compared to FCS or DLS, the lack of scattering issues enabled diffusion measurements in turbid solution (such as blood or plasma) and in gels,[12c] in which scattering of light would have complicated optical detection.

Blood as an important example of a biologically relevant fluid, and as the first one encountered by NPs upon in vivo injection, comprises hundreds of different types of proteins. Despite albumin being the most abundant protein, it is known that other plasma proteins also contribute to the protein corona formation.[11,13] Each of those proteins can adsorb with different kinetics and binding affinities to the surface of NPs forming the so-called protein corona, as outlined generally by Vroman.[14] The binding affinity of different types of proteins to NPs' surfaces can be quantified by the apparent dissociation coefficient K_D'.[15] Protein-concentration dependent measurements of the hydrodynamic radii of NPs upon incubation with proteins allow for determining K_D' using the Hill model.[15b,16] In the present study we explore how generally this principle can be applied to different types of proteins, e.g., what range of K_D' values can be experimentally addressed by the NMR-based detection technique. It is known that the formation of the protein corona is highly dynamic.[17] While temporal resolution of our NMR-based detection may be too slow to follow rearrangements of the protein corona on a minute timescale, this detection certainly would allow for following changes on an hour timescale, which could be relevant for in vitro/in vivo degradation effects of NPs.[18]

The versatility of NMR-based detection methods also allows for multiplexed detection by using different and distinguishable NMR active labels. NMR-based measurements of the hydrodynamic radius of NPs in our set-up are enabled by an organic fluorine (^{19}F) label present in the surface of the NPs. ^{19}F in organic molecules has a spectral width in NMR of about 350 ppm,[19] for which small changes in organic fluorinated compounds can have substantial chemical shifts differences in NMR. Thus, we can take advantage of this property by modifying NPs with different ^{19}F-functionalized ligands leading to differentiated chemical shifts in ^{19}F NMR, based on the used ligand in each case. In this way it is possible to simultaneously measure the hydrodynamic radii of two types of NPs, each modified with a different ^{19}F-functionalized ligand coating.

Nonetheless, the ^{19}F label, due to its high hydrophobicity, may affect the interaction of fluorinated NPs with cells, in particular their endocytotic uptake, as well as potential toxicity. Different degree of ^{19}F labeling thus will not only determine signal intensity of NMR-based detection of hydrodynamic radii, but also potentially changes the properties of the NPs leading to different NP-cell interactions. In order to investigate this effect, in the present study uptake of NPs with different ^{19}F-containing coatings, as well as cell viability, was probed in vitro upon incubation of cultured cells with NPs. The incubation of selected plasma proteins with the fluorinated NPs and their following uptake and cytotoxicity were thus evaluated to obtain feedback for future in vitro and in vivo measurements by magnetic resonance-based technology. This is important to explore the potential of our NMR-based detection of hydrodynamic diameters toward potential in vivo applications.

2. Results

2.1. Synthesis and Characterization of Fluorinated Gold NPs for NMR Diffusion Measurements

Two types of gold NPs functionalized with fluorinated polyethylene glycol (PEG) ligands (HS-PEG-F and HS-PEG-PhF) were synthesized following a reported methodology by us.[12c,20] One of them was additionally coated with amino-ending PEG ligands (HS-PEG-NH_2) and further covered with poly(isobutylene-alt-maleic anhydride) (PMA) polymer, which displays carboxyl groups on its surface when placed in water. This type of NP was selected as a suitable model for protein corona evaluation, based on previous research by us.[12c] For details of the synthesis we refer also to the Supporting Information. The second type of NP was functionalized with a fluorinated PEG ligand bearing a phenyl group (HS-PEG-PhF). Those NPs were named NP-F/NH_2@PMA and NP-PhF, respectively. Transmission electron microscopy (TEM) analysis resulted in core radii values, i.e., the radii of the gold core without organic ligands[21] r_c of 1.8 ± 0.5 nm (NP-F/NH_2@PMA) and 1.6 ± 0.5 nm (NP-PhF). NPs' solution concentrations were obtained by inductively coupled plasma mass spectrometry (ICP-MS) analysis and colloidal stability was verified by ultraviolet-visible spectroscopy.[21] Again, we refer to the Supporting Information for these data. The measured chemical shift of fluorine atoms by ^{19}F NMR was –71.34 ppm and –63.64 ppm for NP-F/NH_2@PMA and NP-PhF, respectively. The so-obtained NMR peaks were single and narrow (≈ 15 Hz of width), maximizing the signal to noise ratio to favor the NMR measurements. That was also reflected in the high transverse relaxation time values (T_2) which were 856 ± 58 and 777 ± 14 ms for NP-F/NH_2@PMA and NP-PhF, respectively. By ^{19}F NMR based diffusion measurements, the diffusion coefficients (D) of NP-F/NH_2@PMA and NP-PhF in PBS were obtained: $D = (1.73 \pm 0.10) \times 10^{-11}$ m^2 s^{-1} and $D = (2.50 \pm 0.02) \times 10^{-11}$ m^2 s^{-1}, respectively. According to the Einstein–Stokes relation, these diffusion coefficients corresponded to the following hydrodynamic radii (r_h):[12c] $r_h = 14.21 \pm 0.84$ nm (NP-F/NH_2@PMA) and $r_h = 9.82 \pm 0.10$ nm (NP-PhF). This increase in hydrodynamic radii as compared to the Au core (i.e., r_h vs r_c) is in line with the ligand shell, which in the case of the PMA-coated NPs is thicker. Detailed characterization is reported in the Supporting Information file.

2.2. Protein Corona Studies from ^{19}F NMR Diffusion Measurements

The increment in size of NP-F/NH_2@PMA due to the presence of a protein corona was studied using ^{19}F NMR based diffusion measurements. Thus, NP-F/NH_2@PMA was separately mixed in phosphate buffered saline (PBS) with increasing concentrations of six different proteins, all of which are present in plasma: bovine serum albumin (BSA), fibrinogen (FIB), apolipoprotein A1 (apoA-I), apolipoprotein E4 (apoE4), apolipoprotein E3 (apoE3), and alpha-2-macroglobulin (α2M). The crystallographic 3D structures of these proteins are depicted in **Figure 1**A (PDB codes for each protein are provided in the Supporting Information). Diffusion coefficients for each

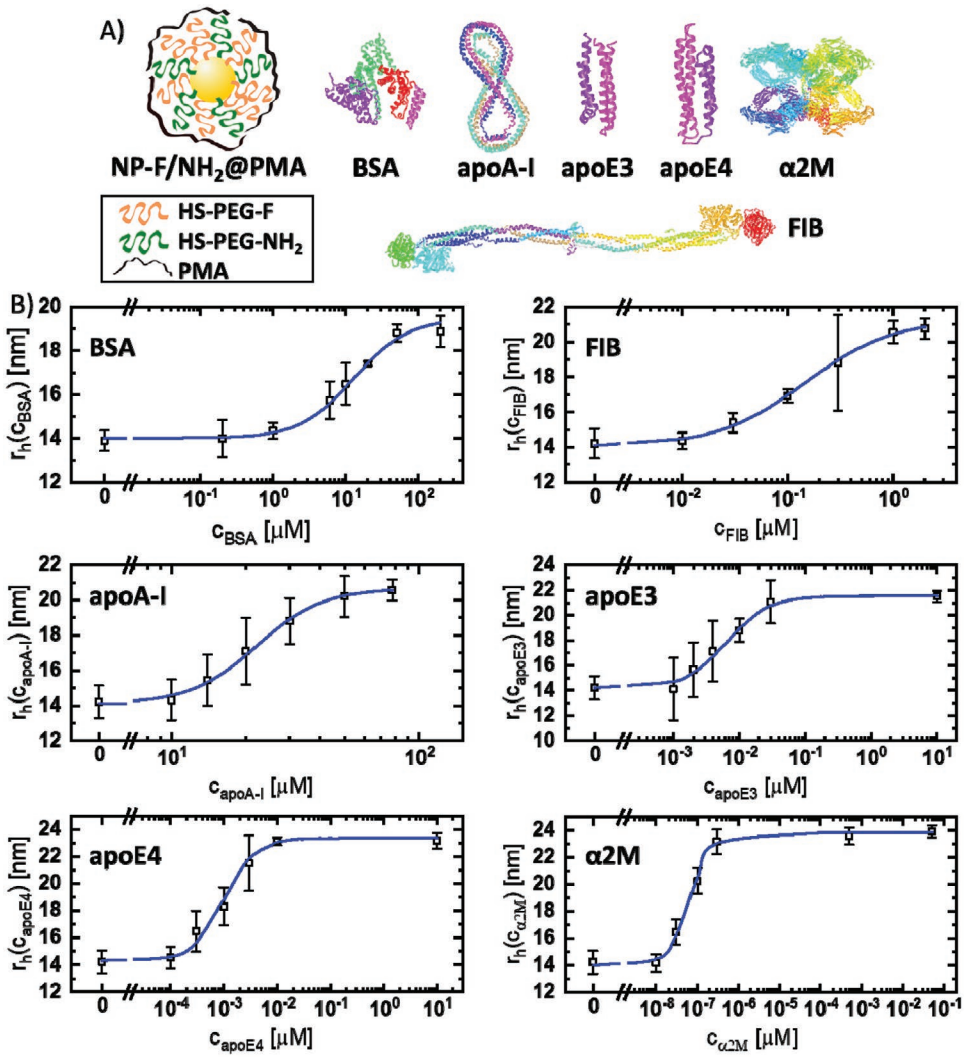

Figure 1. A) Structure of the six proteins investigated in this study. For apoA-I, the tetrameric form is depicted as it is the only reported crystallographic structure. B) Protein concentration c dependent raise in hydrodynamic radius r_h is measured for the six different proteins depicted in (A). The error bars correspond to the standard deviation of 2 to 3 measurements. The blue line represents a fit according to the Hill model. The obtained fit parameters are enlisted in Table 1.

sample were measured by ^{19}F diffusion-based NMR in 5 mm NMR tubes with a coaxial insert loaded with trifluoroacetic acid (TFA) in D_2O. From the diffusion coefficients and applying the Einstein Stokes relation, the hydrodynamic radii (r_h) were calculated. The so-obtained r_h values were plotted against the protein concentration c as employed in each measurement. In all cases a size increase was detected with increasing concentration of each protein up to a saturation point, as it can be seen in Figure 1B. A sigmoidal concentration dependent curve was obtained in all cases and fitted to the Hill model (Figure 1B).[12c] From the fits based on the Hill model it is possible to calculate the apparent dissociation constant (K_D') as an indication of the strength of the interaction between NPs and their corona. The K_D' represents the protein concentration at which half of the NP surfaces are saturated with protein. The fit yields also the Hill coefficient (n), which is related to the cooperativity of the system, the maximum possible number (N_{max}) of proteins attached to the surface of NPs, and the maximum hydrodynamic radius r_h(max) (cf. **Table 1**). The size increment (Δr_h) as observed for each protein after saturation is summarized in Table 1. It ranges from 5.5 ± 0.6 nm for BSA to 9.84 ± 0.49 nm for α2M. In all cases the fitting concluded that all bindings were cooperative ($n > 1$). According to the Hill model, we obtained (K_D') values ranging from (9.1 ± 1.0) × 10^{-14} M for α2M to 24.73 ± 1.17 × 10^{-6} M for apoA-I, which means that we were able to detect events happening at substantially low protein concentrations but also in a wide range of values. These data indicate the huge bandwidth of protein binding to NPs, with dissociation constants spanning nine orders of magnitude in the present case. α2M turns out to be an extremely strong binder, which saturates the NP surface at nine orders of magnitude lower concentrations than apoA-I, which was the weakest binder from the here investigated proteins. The obtained K_D' values are more or less consistent with reported data for PMA coated NPs exposed to either BSA or HSA measured by NMR[12c] or FCS.[22] For the rest of the proteins

Table 1. Fit parameters as obtained for the data shown in Figure 1B after applying the Hill model. $r_h(0)$ is the experimentally obtained value for $c = 0$, whereas $r_h(0)_{(fit)}$ is the value as derived from the fit for $c = 0$. $r_h(max)_{(fit)}$ is the saturation value as obtained from the fit.

Parameters	BSA	FIB	apoA-I	apoE3	apoE4	α2M
$r_h(0)$ [nm]	13.89 ± 0.46	14.21 ± 0.84	14.21 ± 0.84	14.21 ± 0.84	14.21 ± 0.84	14.21 ± 0.84
$r_h(0)_{(fit)}$ [nm]	13.99 ± 0.18	14.05 ± 0.23	14.11 ± 0.15	14.14 ± 0.19	14.25 ± 0.31	13.97 ± 0.32
$r_h(max)_{(fit)}$ [nm]	19.49 ± 0.42	21.30 ± 0.38	20.68 ± 0.13	21.49 ± 0.09	23.48 ± 0.29	23.80 ± 0.17
Δr_h [nm]	5.50 ± 0.60	7.25 ± 0.61	6.57 ± 0.28	7.35 ± 0.28	9.23 ± 0.60	9.84 ± 0.49
K'_D [μM]	17.02 ± 2.89	0.21 ± 0.05	24.73 ± 1.17	0.0087 ± 0.0008	0.0014 ± 0.0003	$(9.1 \pm 1.0) \times 10^{-8}$
N_{max}	110 ± 12	6 ± 1	94 ± 3	120 ± 3	167 ± 8	14 ± 0
n	1.2 ± 0.3	1.1 ± 0.2	3.3 ± 0.4	1.4 ± 0.2	1.5 ± 0.3	1.7 ± 0.2
$A(0)_{(fit)}/N_{max}$ [nm^2]	22	423	27	21	15	181

there is around one order of magnitude of difference between reported data and ours (Table S5, Supporting Information),[22b,d] although there are no available data for all of the tested proteins and comparison is not straightforward due to the different sizes of NPs reported, which may affect the protein adhesion equilibrium.[13] Additionally, it must be taken into account that apolipoproteins are known to self-associate in solution at certain concentration ranges to form dimers, tetramers and even octamers (particularly for apoA-I),[23] for which in our experiments we can foresee competing interactions between self-association of proteins, single protein adhesion to the NP surface and oligomer adhesion to NP surface or to already attached proteins to NPs. A detailed comparison of the here obtained data with literature values can be found in the Supporting Information. For obtaining values for N_{max}, it is required to know the volume that a single protein occupies on the surface of the NP.[15b] For the calculations shown in Table 1 we have used a protein volume (V_P) calculated from the reported stokes radius (r_s) of each protein, and we have assumed that they all behaved as spheres in solution. For comparison purposes, we performed the same calculations by using the reported gyration radius (r_g), the radius derived from the experimentally observed corona thickness (r_Δ) and the V_P obtained from the crystallographic 3D structures (Table S4, Supporting Information). Whenever literature data were available, the volume of associated apolipoproteins in the form of tetramers was also considered for calculations. These calculations led to very different N_{max} values, as proteins differed from a globular shape, and for the case of FIB, which is elongated, the N_{max} varied from 4 to 144 protein units, or in the case of apolipoproteins from a few hundreds to the thousand protein units (Table S4, Supporting Information). Nonetheless, it must be mentioned that in all cases we were assuming that proteins do not change their morphology upon contact with NPs. However, we cannot assess morphological changes or protein denaturation by this methodology. Thus, the values obtained for N_{max} have moderate reliability and in fact in some of the assumptions would be higher that the number of proteins which could actually fit onto the NP surface geometrically in the form of a monolayer. Additionally, and for comparison purposes with other reported systems of different size, we also calculated the area occupied by each protein upon full corona formation (Table 1 and Table S5, Supporting Information). The area occupied by each protein under saturation conditions was obtained by dividing the NP's surface area $A(0) = 4 \cdot \pi \cdot (r_h(0))^2$ by the N_{max} value, and it was mostly in agreement with data reported for other NPs, although big differences were noted for FIB and apoA-I, depending on which N_{max} value was considered (Figure S16, Supporting Information). All detailed data are summarized in Tables S4 and S5 (Supporting Information).

2.3. Multiplexed Studies of Protein Corona from ^{19}F NMR Diffusion Measurements

By using NPs with fluorinated labels with different chemical shift (δ) in ^{19}F NMR, it is possible to monitor the hydrodynamic radii of more than one type of fluorinated NPs in the presence of the same protein. To illustrate this, NP-PhF (δ = –63.64 ppm) was mixed with NP-F/NH_2@PMA (δ = –71.34 ppm) in PBS in the presence of a fixed concentration of α2M (0.05×10^{-6} M). NMR diffusion measurements were performed as described before in a 5 mm NMR tube with a coaxial insert carrying TFA in deuterated water. Since the signals from each type of NPs are sufficiently apart ($\Delta\delta \approx 8$ ppm), it is possible to analyze the intensity decay in the NMR spectra of each NP independently. Thus, the obtained values for the diffusion coefficient D for each type of NPs in the presence of α2M were $(1.02 \pm 0.01) \times 10^{-11}$ m^2 s^{-1} and $(2.21 \pm 0.11) \times 10^{-11}$ m^2 s^{-1} for NP-F/NH_2@PMA and NP-PhF, respectively. Those D values correspond to r_h values of 24.15 ± 0.17 nm (NP-F/NH_2@PMA) and 11.09 ± 0.53 nm (NP-PhF), and the Δr_h values were 9.94 ± 1.01 and 1.27 ± 0.63 nm for NP-F/NH_2@PMA and NP-PhF, respectively, see **Figure 2**. Hence, while NP-F/NH_2@PMA was totally coated with α2M, NP-PhF barely interacted with the same protein concentration. This could be explained by the very different surface of both NPs, one of them coated with PMA, a polycarboxylated polymer, and the other one coated with fluorinated phenyl moieties. These data clearly demonstrate that the here reported methodology can be applied to observe in situ the hydrodynamic radii over several NP types in the same environment in a multiplexed way, allowing for example for direct comparison and/or integration of control NPs.

2.4. NP Synthesis for Cellular Cytotoxicity and Uptake Studies

Fluorinated (NP-F) and non-fluorinated NPs (NP-OH), combined or not with carboxyl (NP-F/COOH and NP-OH/COOH)

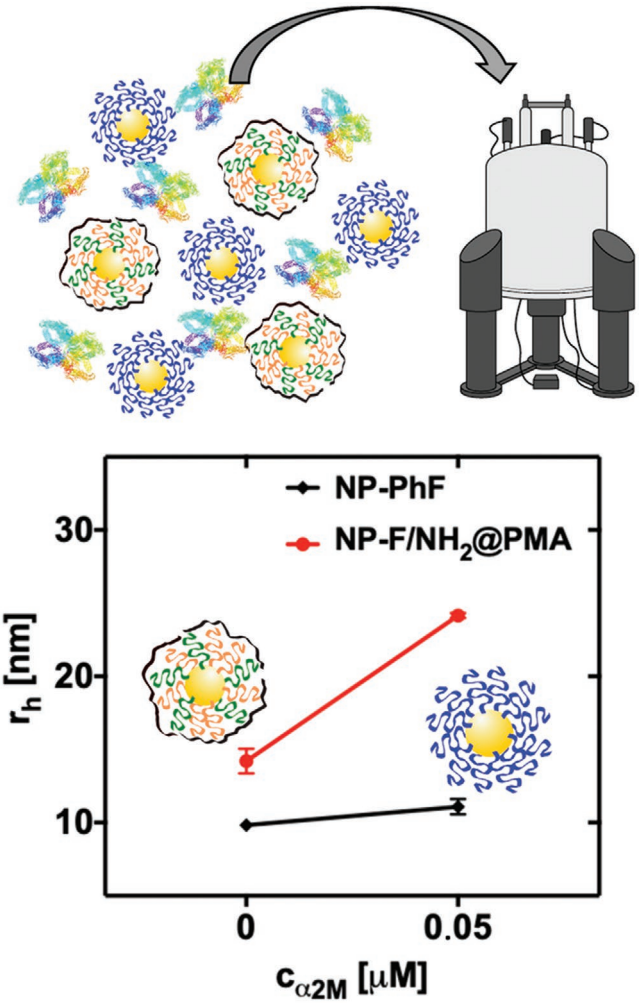

Figure 2. Two different types of NPs (NP-PhF and NP-F/NH_2@PMA) were exposed simultaneously in the same vessel to different concentrations c of α2M. Due to the different fluorine labels, the hydrodynamic radii r_h of both types of NPs could be detected simultaneously, demonstrating the feasibility of multiplexed measurements.

or amino (NP-F/NH_2 and NP-OH/NH_2) ending PEG ligands were prepared to study the influence of fluorine content, surface charge, and hydrophobicity of the NPs on NP uptake by cells and potential influence on cell viability. NP-F contained 100% of fluorinated ligands, NP-F/COOH and NP-F/NH_2 had 65% of fluorine ligands and NP-OH, NP-OH/COOH, and NP-OH/NH_2 had 0% of fluorine content. These NPs were prepared following the same procedure as already described by us.[12c,20] TEM analysis showed r_c values ranging from 1.5 ± 0.5 to 1.9 ± 0.7 nm for all six types of NPs (we refer to the Supporting Information for the raw data). Regarding their zeta potential NP-F, NP-OH, NP-F/COOH, and NP-OH/COOH are negatively charged with zeta potential values ζ between −24.0 ± 0.7 and −8.6 ± 0.1 mV and NP-F/NH_2 and NP-OH/NH_2 are positively charged with zeta potential values of 25.0 ± 0.9 and 15.6 ± 0.4 mV, respectively. Interfacial tension (IFT) measurements[24] were performed with all six types of NPs to assess hydrophobicity and the following trend from higher to lower hydrophobicity was observed: NP-F ≈ NP-F/NH_2 > NP-F/COOH > NP-OH ≈ NP-OH/COOH ≈ NP-OH/NH_2. Detailed synthetic and characterization data are reported in the Supporting Information file.

2.5. Cell Viability and Uptake Assays: Influence of Fluorine Label

HeLa cells (7.5×10^3 cells per well) were independently exposed to the different types of NPs in NP concentrations c_{NP} (these are not elemental concentrations, but NP concentrations[21]) ranging from 0 to 1.75×10^{-7} M. Exposure was carried out for either 24 or 48 h, both in the presence and absence of fetal bovine serum (FBS), to also take into account the protein corona influence. It was observed that none of the NPs reduced cell viability under the given exposure conditions, independently from the NP surface or concentration, FBS presence or absence and incubation time. This demonstrates that the presence of the ^{19}F label does not impose additional toxicity which would prevent diffusion coefficient measurements in the presence of cells. Concerning potential use of the NPs with ^{19}F label for measuring protein adsorption in vitro/in vivo, two scenarios need to be differentiated. First, for measurements inside cells the NPs should be internalized. However, endocytosis may induce agglomeration of the NPs inside intracellular vesicles, and thus this route still needs to be explored. Second, protein corona formation could be potentially measured in vivo in blood. In this scenario the NPs should have long circulations times, i.e., should not be internalized by cells (e.g., macrophages). Here we explore the 2nd strategy, in which the uptake of NPs by cells should be as low as possible, and whether the degree of ^{19}F labeling plays any role. Subsequently, cellular uptake studies were performed and quantified by ICP-MS analysis of incubated cells with NPs (**Figure 3**). For uptake experiments, HeLa cells (2.2×10^5 cells per well) were incubated separately with each type of NP at either 5×10^{-8} or 1×10^{-7} M of NP concentration, in the presence or absence of FBS and for 24–48 h. In all cases it was noticed that uptake increased with increasing NP concentration (5×10^{-8} vs 1×10^{-7} M), and it also increased with exposure time (24 vs 48 h). Those differences were more noticeable in the absence of FBS, where the surface of NPs is exposed due to the absence of protein corona, in line with the general believe that differences in surface chemistry are "smeared-out" in serum containing medium.[25] Nonetheless, the uptake for all 6 types of NPs was relatively low as compared to other NPs[26] and was below 0.5 pg per cell in all cases. This is due to the PEG coating, which involves lower NP internalization than for PMA-coated NPs.[2,27] There was no stunning effect due to the ^{19}F labeling. Usually, positively charged NPs are reported to be internalized more than neutral or negatively charged ones due to increased interaction with the negatively charged cell membrane. However, in our case, no differences in uptake were observed due to differences in charge, with or without ^{19}F label. This effect however can strongly depend on the used cells and it is often not as evident as generally believed.[25] Some small contribution from hydrophobicity was detected, though. Indeed, the highest uptake was recorded for NP-F (1×10^{-7} M) incubated for 48 h in the absence of FBS. At 5×10^{-8} M concentration, NP-F was also the most internalized NP, but with little difference with respect to the others. However, in the presence

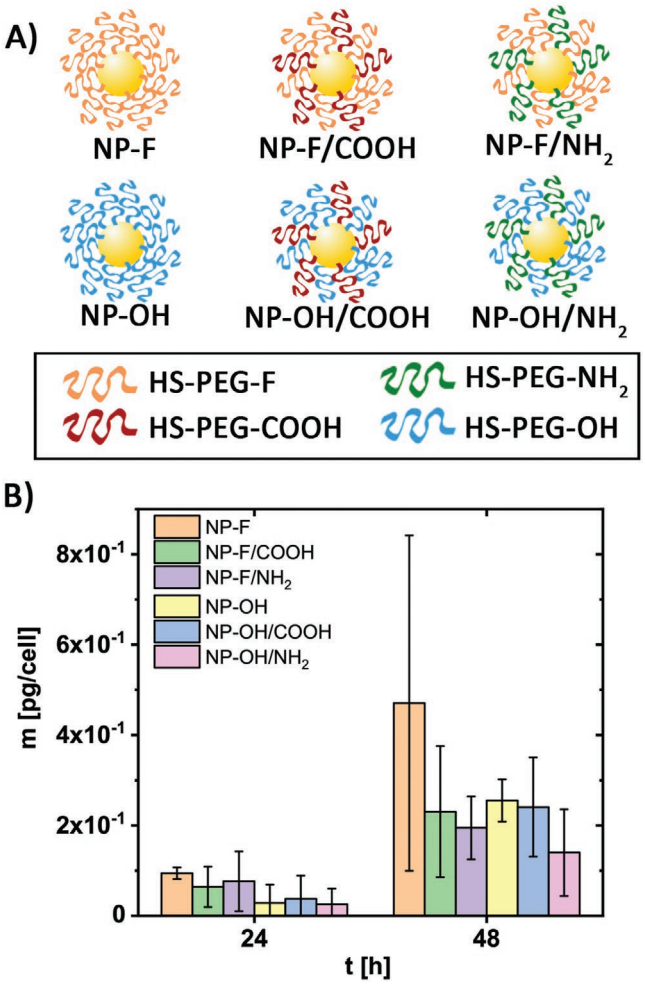

Figure 3. A) Illustration of the fluorinated (NP-F, NP-F/COOH, and NP-F/NH_2) and nonfluorinated NPs (NP-OH, NP-OH/COOH, and NP-OH/NH_2) used for cellular uptake and cytotoxicity assays. B) Amount of internalized NPs per cell m [pg per cell] upon exposure of HeLa cells for $t = 24$ or 48 h to different types of NPs at NP exposure concentration of 1×10^{-7} M in serum free medium.

of FBS the highest uptake was for NP-F/NH_2 (1×10^{-7} M) incubated for 48 h. According to our IFT measurements (see the Supporting Information) both, NP-F and NP-F/NH_2 are the most hydrophobic NPs with very similar values of interfacial tension. There is always the discussion to which extend labeling interferes with the physicochemical properties of NPs. Our data here demonstrate that ^{19}F labeling may moderately affect interaction of NPs with cells, which needs to be considered while interpreting results of diffusion coefficient measurements.

3. Discussion

In this work the ^{19}F NMR-based methodology to measure protein corona[12c] has been extended to relevant plasma proteins. As for other methods used to study formation of the protein corona based on changes in hydrodynamic diameter of the NPs, our methodology does not provide information at a molecular level. For this, mass spectrometry-based analysis is needed, which however in particular in the case of in vivo measurements required extraction and purification of the NP sample.[3] In the case of concentration-dependent size measurements the fitting of the data to the Hill model can only give a rough estimation and perhaps a rather simplistic interpretation of the protein adhesion equilibrium. On the one hand, the K_D' values, representing the protein concentration at which half of the NP surface is covered with proteins, can be obtained experimentally from the measured data as the half point of the curve and can be interpreted directly. However, uncertainties such as the protein 3D structure once adsorbed onto the NPs' surface or the association state of apolipoproteins in solution, makes that fitting parameters such as the Hill coefficient or the N_{max} value can only be interpreted roughly because of the complexity of the system. Indeed, we cannot assume that there is only one type of interaction, i.e., NP-protein, at play. Competing interactions between single apolipoproteins, protein oligomers, and NPs are undetectable by our methodology and therefore cannot be considered in the data analysis. Also, we cannot rule out that there could be (small) patches of NP-F/NH_2@PMA that may not be fully coated with PMA, exposing some of the PEGylated fluorinated ligands. This will also complicate the data analysis because different types of interactions with the same protein may take place on the surface of each NP.

The presence of a fluorine label enables the measurement of diffusion coefficients of fluorinated NPs in the presence of plasma proteins, which naturally lack fluorine. Cytotoxicity and uptake studies suggest that the fluorine label does not have a great impact on the uptake of NPs by HeLa cells and the internalization is very low as expected for PEGylated NPs irrespective of the overall charge. Hydrophobic NP-F and NP-F/NH_2 had slightly greater uptake than the rest of NPs, although still low. The low internalization may account for the lack of toxicity at all of the concentrations tested. No big differences were detected when incubations were performed either in the presence or absence of FBS, although in the presence of serum the internalization rate was in general lower than in its absence. Nonetheless, proteins such as fibrinogen are not present in FBS because the blood is clotted before serum collection and the fibrin containing clot removed.[28] However, hydrophobic proteins seem to interact strongly with hydrophobic NPs as we observed in previous studies by incubating NP-F and NP-F/NH_2 with FIB[12c] for which the contribution from hydrophobicity is not fully assessed.

4. Conclusion

In conclusion, we have proven that our NMR-based methodology can be extended to observe the protein corona formation over six relevant plasma proteins in situ, that is, in equilibrium with excess unbound proteins. Relevant data regarding the increase in hydrodynamic radii due to the presence of a protein corona and the affinity of each protein toward the NP's surface can be obtained from our analysis and have been characterized for each protein. The use of ^{19}F labels on our NPs enables the in situ measurements benefiting from the natural absence of fluorine in plasma proteins. Combining different fluorine labels, it has been possible to measure the interaction of one protein

at a fixed concentration with two different NPs. Such fluorine label does not have a cytotoxic effect on HeLa cells most likely due to the low internalization detected by ICP-MS analysis of lysed cells. Most importantly, as this NMR-based detection is not subject to absorption/scattering effects of tissue, it could be potentially employed under optically non-transparent conditions, which is a requirement for potential future in vivo application.

5. Experimental Section

Diffusion Measurements in the Presence of Proteins by ^{19}F NMR and Size Calculation: All NMR data were collected on a Bruker AVANCE III NMR spectrometer (11.7 T, 470.59 MHz for ^{19}F) equipped with a 5 mm $^{1}H/^{19}F$ BBI probe with actively shielded *z*-gradient that was used in combination with a Bruker gradient amplifier providing a maximum current of 10 A, which results in a maximum 56 G cm^{-1} gradient. NP ($c_{NP} \geq 0.5 \times 10^{-6}$ M) and protein mixtures (465 µL) of known concentrations were placed in 5 mm standard NMR tubes with a coaxial insert carrying TFA in D_2O (0.024% v/v) as a reference for chemical shift. ^{19}F diffusion NMR measurements were performed using stimulated echo with bipolar gradient pulses from Bruker's sequence library (stebpgp1s) with the following parameters: 4k acquisition points, SW 15 ppm, NS ≥ 480, DS 32, D1 2 s, D20 (gradient length) 0.6 s, P30 (diffusion delay/2) 2.0 ms, and 12 equally spaced gradient strengths from 5 to 95%. NMR measurements were performed using deuterium lock at 25 °C. Diffusion spectra were analyzed using Mnova 12.0 software. Full details with the concentrations used for each experiment are displayed in the Supporting Information. As in a previous work,[12c] diffusion constants for each sample were calculated by fitting the NMR signal intensity (I) decay to a monoexponential decay equation with the scaling factor B with or without an off-set A ($I = A + B \cdot e^{-D \cdot Z}$), where I is directly measured on the NMR spectra, the diffusion constant (D) is obtained from the fitting and Z corresponds to the Z values, i.e., the gradient strengths scaled according to the Tanner–Stejskal model ($Z = (\gamma \delta G)^2(\Delta - \delta/3)$) being γ [Hz T^{-1}] the gyromagnetic ratio of ^{19}F, δ [s] the gradient length, Δ [s] the diffusion delay, and G [T m^{-1}] the gradient strength. Subsequently, the hydrodynamic radii r_h for each NP sample were calculated using the diffusion constant D and applying the Einstein–Stokes relation, assuming spherical shape for NPs ($r_h = k_B T/(6\pi\eta D)$), where, r_h is the hydrodynamic radius, η is the dynamic viscosity, T is the absolute temperature in Kelvin, D is the diffusion constant, and k_B is the Boltzmann constant. All experimental procedures are detailed in the Supporting Information.

Supporting Information

Supporting Information is available from the Wiley Online Library or from the author.

Acknowledgements

This work was supported by the Cluster of Excellence "Advanced Imaging of Matter" of the Deutsche Forschungsgemeinschaft (DFG) – EXC 2056 – project ID 390715994, by the Basque Government (project IT1196-19) and by the Fundación Biofísica Bizkaia and the Basque Excellence Research Centre (BERC) program of the Basque Government. This work was performed under the Maria de Maeztu Units of Excellence Programme—Grant No. MDM-2017-0720 Ministry of Science, Innovation and Universities. The help of Marta Gallego in the surface tension and TEM measurements is acknowledged. Parts of the ICP-MS measurements were done at the ICP-MS facility of CIC biomaGUNE by Javier Calvo.

Conflict of Interest

The authors declare no conflict of interest.

Keywords

fluorinated nanoparticles, in situ, NMR, plasma proteins, protein corona

Received: February 23, 2020
Revised: April 16, 2020
Published online: May 19, 2020

[1] a) T. Cedervall, I. Lynch, S. Lindman, T. Berggård, E. Thulin, H. Nilsson, K. A. Dawson, S. Linse, *Proc. Natl. Acad. Sci. USA* **2007**, *104*, 2050; b) I. Lynch, T. Cedervall, M. Lundqvist, C. Cabaleiro-Lago, S. Linse, K. A. Dawson, *Adv. Colloid Interface Sci.* **2007**, *134–135*, 167; c) I. Lynch, K. A. Dawson, *Nano Today* **2008**, *3*, 40.

[2] D. Hühn, K. Kantner, C. Geidel, S. Brandholt, I. De Cock, S. J. H. Soenen, P. Rivera Gil, J.-M. Montenegro, K. Braeckmans, K. Müllen, G. U. Nienhaus, M. Klapper, W. J. Parak, *ACS Nano* **2013**, *7*, 3253.

[3] M. Hadjidemetriou, Z. Al-Ahmady, M. Mazza, R. F. Collins, K. Dawson, K. Kostarelos, *ACS Nano* **2015**, *9*, 8142.

[4] a) P. Grenier, I. M. d. O. Viana, E. M. Lima, N. Bertrand, *J. Controlled Release* **2018**, *287*, 121; b) D. Bargheer, J. Nielsen, G. Gebel, M. Heine, S. C. Salmen, R. Stauber, H. Weller, J. Heeren, P. Nielsen, *Beilstein J. Nanotechnol.* **2015**, *6*, 36; c) C. Gunawan, M. Lim, C. P. Marquis, R. Amal, *J. Mater. Chem. B* **2014**, *2*, 2060.

[5] a) D. Westmeier, C. Chen, R. H. Stauber, D. Docter, *Eur. J. Nanomed.* **2016**, *7*, 153; b) D. Westmeier, R. H. Stauber, D. Docter, *Toxicol. Appl. Pharmacol.* **2016**, *299*, 53.

[6] S. Balog, L. Rodriguez-Lorenzo, C. A. Monnier, M. Obiols-Rabasa, B. Rothen-Rutishauser, P. Schurtenberger, A. Petri-Fink, *Nanoscale* **2015**, *7*, 5991.

[7] A. A. Sousa, *J. Fluoresc.* **2015**, *25*, 1567.

[8] K. Fischer, M. Schmidt, *Biomaterials* **2016**, *98*, 79.

[9] a) L. Shang, G. U. Nienhaus, *Acc. Chem. Res.* **2017**, *50*, 387; b) G. U. Nienhaus, P. Maffre, K. Nienhaus, *Methods Enzymol.* **2013**, *519*, 115; c) X. Jiang, S. Weise, M. Hafner, C. Röcker, F. Zhang, W. J. Parak, G. U. Nienhaus, *J. R. Soc., Interface* **2010**, *7*, S5.

[10] W. Liu, J. Rose, S. Plantevin, M. Auffan, J. Y. Bottero, C. Vidaud, *Nanoscale* **2013**, *5*, 1658.

[11] H. Wang, L. Shang, P. Maffre, S. Hohmann, F. Kirschhöfer, G. Brenner-Weiß, G. U. Nienhaus, *Small* **2016**, *12*, 5836.

[12] a) C. Zhang, G. Palui, B. Zeng, N. Zhan, B. Chen, H. Mattoussi, *Chem. Mater.* **2018**, *30*, 3454; b) B. Zeng, G. Palui, C. Zhang, N. Zhan, W. Wang, X. Ji, B. Chen, H. Mattoussi, *Chem. Mater.* **2018**, *30*, 225; c) M. Carril, D. Padro, P. d. Pino, C. Carrillo-Carrion, M. Gallego, W. J. Parak, *Nat. Commun.* **2017**, *8*, 1542; d) C. Porsch, Y. N. Zhang, A. Ostlund, P. Damberg, C. Ducani, E. Malmstrom, A. M. Nystrom, *Part. Part. Syst. Charact.* **2013**, *30*, 381; e) C. Zhang, Z. Jin, B. Zeng, W. Wang, G. Palui, H. Mattoussi, *J. Phys. Chem. B* **2020**, https://doi.org/10.1021/acs.jpcb.0c02177.

[13] S. Tenzer, D. Docter, S. Rosfa, A. Wlodarski, J. Kuharev, A. Rekik, S. K. Knauer, C. Bantz, T. Nawroth, C. Bier, J. Sirirattanapan, W. Mann, L. Treuel, R. Zellner, M. Maskos, H. Schild, R. H. Stauber, *ACS Nano* **2011**, *5*, 7155.

[14] a) L. Vroman, A. Lukosevicius, *Nature* **1964**, *204*, 701; b) S. L. Hirsh, D. R. McKenzie, N. J. Nosworthy, J. A. Denman, O. U. Sezerman, M. M. M. Bilek, *Colloids Surf., B* **2013**, *103*, 395; c) S.-Y. Jung, S.-M. Lim, F. Albertorio, G. Kim, M. C. Gurau, R. D. Yang, M. A. Holden, P. S. Cremer, *J. Am. Chem. Soc.* **2003**, *125*, 12782.

[15] a) A. V. Orlov, J. A. Khodakova, M. P. Nikitin, A. O. Shepelyakovskaya, F. A. Brovko, A. G. Laman, E. V. Grishin, P. I. Nikitin, *Anal. Chem.* **2013**, *85*, 1154; b) P. del_Pino, B. Pelaz, Q. Zhang, P. Maffre, G. U. Nienhaus, W. J. Parak, *Mater. Horiz.* **2014**, *1*, 301.
[16] a) A. V. Hill, T. G. Brown, H. E. Roaf, *J. Physiol.* **1910**, *40*, i; b) L. Endrenyi, C. Fajszi, F. H. F. Kwong, *Eur. J. Biochem.* **1975**, *51*, 317.
[17] a) S. Tenzer, D. Docter, J. Kuharev, A. Musyanovych, V. Fetz, R. Hecht, F. Schlenk, D. Fischer, K. Kiouptsi, C. Reinhardt, K. Landfester, H. Schild, M. Maskos, S. K. Knauer, R. H. Stauber, *Nat. Nanotechnol.* **2013**, *8*, 772; b) E. Casals, T. Pfaller, A. Duschl, G. J. Oostingh, V. F. Puntes, *Small* **2011**, *7*, 3479; c) E. Casals, T. Pfaller, A. Duschl, G. J. Oostingh, V. F. Puntes, *ACS Nano* **2010**, *4*, 3623.
[18] a) W. G. Kreyling, A. M. Abdelmonem, Z. Ali, F. Alves, M. Geiser, N. Haberl, R. Hartmann, S. Hirn, D. J. de Aberasturi, K. Kantner, G. Khadem-Saba, J. M. Montenegro, J. Rejman, T. Rojo, I. R. de Larramendi, R. Ufartes, A. Wenk, W. J. Parak, *Nat. Nanotechnol.* **2015**, *10*, 619; b) C. Carrillo-Carrion, A. I. Bocanegra, B. Arnaiz, N. Feliu, D. Zhu, W. J. Parak, *ACS Nano* **2019**, *13*, 4631.
[19] W. R. Dolbier Jr., *Guide to Fluorine NMR for Organic Chemists*, John Wiley & Sons, New York **2016**.
[20] O. Michelena, D. Padro, C. Carrillo-Carrión, P. d. Pino, J. Blanco, B. Arnaiz, W. J. Parak, M. Carril, *Chem. Commun.* **2017**, *53*, 2447.
[21] J. Hühn, C. Carrillo-Carrion, M. G. Soliman, C. Pfeiffer, D. Valdeperez, A. Masood, I. Chakraborty, L. Zhu, M. Gallego, Y. Zhao, M. Carril, N. Feliu, A. Escudero, A. M. Alkilany, B. Pelaz, P. d. Pino, W. J. Parak, *Chem. Mater.* **2017**, *29*, 399.
[22] a) J. Hühn, C. Fedeli, Q. Zhang, A. Masood, P. d. Pino, N. M. Khashab, E. Papini, W. J. Parak, *Int. J. Biochem. Cell Biol.* **2016**, *75*, 148; b) P. Maffre, K. Nienhaus, F. Amin, W. J. Parak, G. U. Nienhaus, *Beilstein J. Nanotechnol.* **2011**, *2*, 374; c) C. Röcker, M. Pötzl, F. Zhang, W. J. Parak, G. U. Nienhaus, *Nat. Nanotechnol.* **2009**, *4*, 577; d) B. Pelaz, P. Del Pino, P. Maffre, R. Hartmann, M. Gallego, S. Rivera-Fernandez, J. M. de la Fuente, G. U. Nienhaus, W. J. Parak, *ACS Nano* **2015**, *9*, 6996; e) P. Maffre, S. Brandholt, K. Nienhaus, L. Shang, W. J. Parak, G. U. Nienhaus, *Beilstein J. Nanotechnol.* **2014**, *5*, 2036; f) S. Dominguez-Medina, S. McDonough, P. Swanglap, C. F. Landes, S. Link, *Langmuir* **2012**, *28*, 9131.
[23] a) H.-J. Schönfeld, D. Roessner, J. Seelig, *J. Phys. Chem. B* **2016**, *120*, 1228; b) K. Garai, C. Frieden, *Biochemistry* **2010**, *49*, 9533.
[24] P. del_Pino, F. Yang, B. Pelaz, Q. Zhang, K. Kantner, R. Hartmann, N. M. d. Baroja, M. Gallego, M. Möller, B. B. Manshian, S. J. Soenen, R. Riedel, N. Hampp, W. J. Parak, *Angew. Chem., Int. Ed.* **2016**, *55*, 5483.
[25] S. Ashraf, A. H. Said, R. Hartmann, M.-A. Assmann, N. Feliu, P. Lenz, W. J. Parak, *Angew. Chem.* **2020**, *59*, 5438.
[26] X. Sun, M. Gamal, P. Nold, A. Said, I. Chakraborty, B. Pelaz, F. Schmied, K. v. Pückler, J. Figiel, Y. Zhao, C. Brendel, M. Hassan, W. J. Parak, N. Feliu, *Appl. Mater. Today* **2019**, *15*, 267.
[27] M. Xu, M. G. Soliman, X. Sun, B. Pelaz, N. Feliu, W. J. Parak, S. Liu, *ACS Nano* **2018**, *12*, 10104.
[28] M. Johnson, *Mater. Methods* **2012**, *2*, 117.